ANL/ASD/CP-97292

Development of a 3D FEL code for the simulation of a high-gain harmonic generation experiment

S.G. Biedron[a], H.P. Freund[b], and S.V. Milton[a]
[a]Advanced Photon Source, Argonne National Laboratory, Argonne, IL 60439
[b]Science Applications International Corp., McLean, VA 22102

SPIE paper # 3614 17

Free-Electron Laser Challenges II, part of SPIE's Photonics West '99
January 23-29, 1999
San Jose, CA

DISCLAIMER

Development of a 3D FEL code for the simulation of a high-gain harmonic generation experiment

S.G. Biedron*[a], H.P. Freund[b], and S.V. Milton[a]
[a]Advanced Photon Source, Argonne National Laboratory, Argonne, IL 60439
[b]Science Applications International Corp., McLean, VA 22102

ABSTRACT

Over the last few years, there has been a growing interest in self-amplified spontaneous emission (SASE) free-electron lasers (FELs) as a means for achieving a fourth-generation light source. In order to correctly and easily simulate the many configurations that have been suggested, such as multi-segmented wigglers and the method of high-gain harmonic generation, we have developed a robust three-dimensional code. The specifics of the code, the comparison to the linear theory as well as future plans will be presented.

Keywords : FEL, Free-Electron Laser, SASE, Self-Amplified Spontaneous Emission, MEDUSA, numerical simulation, APS SASE FEL, High-Gain Harmonic Generation

1. INTRODUCTION

With the growing interest in free-electron laser (FEL) physics, particularly in the self-amplified spontaneous emission (SASE) regime for both a proof-of-principle experiment and an actual fourth-generation light source, many simulation codes have been developed.[1] Among these, the FEL simulation code MEDUSA has evolved to handle a variety of applications.[2] Most recently we have included Gaussian and waterbag distributions with energy spread, multiple-segment wigglers (with the capability of using different wiggler periods, if desired), multiple frequencies (harmonics and bandwidth), additional beam diagnostics, as well as quadrupole focusing and dipoles. Here we discuss MEDUSA's capabilities in detail, as well as the results from the simulation runs based on the APS SASE FEL's parameters[3] compared to the linear theory,[4] the observation of nonlinear harmonic generation,[5] and the plan to use MEDUSA in the simulation of applications such as a high-gain harmonic generation experiment.[6]

2. MEDUSA'S CAPABILITIES

In the simulation code MEDUSA the electromagnetic field is represented as a superposition of Gauss-Hermite optical modes, whose vector potential is defined as

$$\delta\mathbf{A}(\mathbf{x},t)=\hat{\mathbf{e}}_x\sum_{l,n,h}e_{l,n,h}(x,y)\left[\delta A^{(1)}_{l,n,h}\cos\varphi_h+\delta A^{(2)}_{l,n,h}\sin\varphi_h\right]\ . \tag{1}$$

Here, l and n denote the transverse mode numbers, h denotes the harmonic number, and

$$e_{l,n,h}(x,y)=\exp\left(-r^2/w_h^2\right)H_l\left(\sqrt{2}\,x/w_h\right)H_n\left(\sqrt{2}\,y/w_h\right), \tag{2}$$

where H_l and H_n are the Hermite polynomials of order l and n, respectively, and w_h is the spot size of the h^{th} harmonic component. The vacuum phase is given by

$$\varphi_h=h(k_0z-\omega_0t)+\alpha_h r^2/w_h^2\,, \tag{3}$$

for the vacuum wavenumber k_0 (= ω_0/c), where α_h is related to the curvature of the phase front. An expansion in vacuum modes is accomplished by using the vacuum solutions for the mode waists and curvatures. These solutions are then expressed as

* Correspondence: Email: biedron@aps.anl.gov, Telephone: 630 252 1162, Fax: 630 252 5703

$$w_h = w_h(z=0)\left[1+z^2/z_{0h}^2\right]^{1/2} \tag{4}$$

and

$$\alpha_h = z/z_{0h} \tag{5}$$

where $z_{0h} = hk_0 w_h^2(z=0)/2$ is the Rayleigh range. The one drawback to this approach is that a large number of Gauss-Hermite modes are required to accurately describe the optical guiding of the radiation. In another approach, using a source-dependent expansion (SDE) technique re-derived for the Gauss-Hermite representation of the three-dimensional radiation field,[7] the radiation field is accurately described with a small number of optical modes while still maintaining the existence of accurately represented optical guiding. This has significantly reduced MEDUSA's run times.

In MEDUSA, the field equations are integrated simultaneously with the three-dimensional Lorentz force equations for a planar wiggler geometry for some number of electrons. The dynamical equations for the field are

$$\left(\frac{d}{dz}+\frac{w_h'}{w_h}\right)\begin{pmatrix}\delta a_{l,n,h}^{(1)}\\ \delta a_{l,n,h}^{(2)}\end{pmatrix}+K_{l,n,h}\begin{pmatrix}\delta a_{l,n,h}^{(2)}\\ -\delta a_{l,n,h}^{(1)}\end{pmatrix}=\begin{pmatrix}s_{l,n,h}^{(1)}\\ s_{l,n,h}^{(2)}\end{pmatrix}, \tag{6}$$

where $\delta a_{l,n,h}^{(i)} = e\delta A_{l,n,h}^{(i)}/m_e c^2$ are the normalized amplitudes (i = 1,2), the "prime" superscript denotes a z-derivative,

$$K_{l,n,h} = (l+n+1)\left(\alpha_h\frac{w_h'}{w_h}-\frac{\alpha_h'}{2}-\frac{1+\alpha_h^2}{hk_0w_h^2}\right), \tag{7}$$

and

$$\begin{pmatrix}s_{l,n,h}^{(1)}\\ s_{l,n,h}^{(2)}\end{pmatrix}=\frac{2\omega_b^2}{h\omega_0 c}\frac{1}{2^{l+n}\,l!n!w_h^2}\left\langle\frac{v_x}{|v_z|}e_{l,n,h}\begin{pmatrix}\cos\varphi_h\\ -\sin\varphi_h\end{pmatrix}\right\rangle, \tag{8}$$

where $\omega_h^2 = 4\pi e^2 n_b/m_e$ is the square of the plasma frequency, n_b is the particle density, and v_x and v_z are the particle velocities in the x and z directions. For a beam with a uniform temporal profile and Gaussian energy and phase space distributions, the source terms are

$$\langle\langle(\cdots)\rangle\rangle = \int_0^{2\pi}\frac{d\psi_0}{2\pi}\int_0^{\infty}d\gamma_0\,\frac{\exp\left[-(\gamma_0-\bar{\gamma}_0)^2/2\Delta\gamma^2\right]}{\sqrt{\pi/2}\Delta\gamma\left[1+\mathrm{erf}\left(\bar{\gamma}_0/\sqrt{2}\Delta\gamma\right)\right]}$$

$$\times\iiiint dx_0dy_0dp_{x0}dp_{y0}\,\frac{\exp\left(-r_0^2/2\sigma_r^2-p_{\perp0}^2/2\sigma_p{}^2\right)}{(2\pi)^2\sigma_r^2\sigma_p{}^2}(\cdots)\ , \tag{9}$$

where the average is over the initial beam parameters (denoted by the subscript "0") in ponderomotive phase ($\psi_0 = -\omega_0 t_0$), energy (γ_0), and phase space (x_0,y_0,p_{x0},p_{y0}); $\bar{\gamma}_0$ and $\Delta\gamma$ denote the average beam energy and the energy spread; and σ_r and σ_p describe the initial phase space parameters. For a matched beam, we require that

$$\sigma_r = \sqrt{\frac{\beta\varepsilon_n}{\bar{\gamma}_0}}\quad\text{and}\quad\sigma_p = \sqrt{\frac{\bar{\gamma}_0\varepsilon_n}{\beta}}\ , \tag{10}$$

where $\beta = \gamma / a_w k_w$, is the beam beta-function.

The utility of the SDE is that the diffraction of each harmonic component is governed by

$$\frac{w_h'}{w_h} = \frac{2\alpha}{hk_0 w_h^2} - Y_h, \tag{11}$$

$$\frac{\alpha_h'}{2} = \frac{1+\alpha_h^2}{hk_0 w_h^2} - (X_h + \alpha_h Y_h), \tag{12}$$

where X_h and Y_h are defined in terms of the source terms as

$$X_h = 2\frac{\left(s_{2,0,h}^{(1)} + s_{0,2,h}^{(1)}\right)\delta a_{0,0,h}^{(2)} - \left(s_{2,0,h}^{(2)} + s_{0,2,h}^{(2)}\right)\delta a_{0,0,h}^{(1)}}{\delta a_{0,0,h}^2}, \tag{13}$$

$$Y_h = -2\frac{\left(s_{2,0,h}^{(1)} + s_{0,2,h}^{(1)}\right)\delta a_{0,0,h}^{(1)} + \left(s_{2,0,h}^{(2)} + s_{0,2,h}^{(2)}\right)\delta a_{0,0,h}^{(2)}}{\delta a_{0,0,h}^2}, \tag{14}$$

and $\delta a_{0,0,h}^2 = \delta a_{0,0,h}^{(1)\,2} + \delta a_{0,0,h}^{(2)\,2}$. In the absence of the electron beam, $X_h = Y_h = 0$, we recover vacuum diffraction given by Eqs. (4) and (5).

There are two wiggler models included in MEDUSA. The parabolic-pole-face (PPF) wiggler model is defined as

$$\mathbf{B}_w = B_w\left\{\cos k_w z\left[\hat{\mathbf{e}}_x \sinh\left(\frac{k_w x}{\sqrt{2}}\right)\sinh\left(\frac{k_w y}{\sqrt{2}}\right) + \hat{\mathbf{e}}_y \cosh\left(\frac{k_w x}{\sqrt{2}}\right)\cosh\left(\frac{k_w y}{\sqrt{2}}\right)\right]\right.$$
$$\left. - \sqrt{2}\hat{\mathbf{e}}_z \sin k_w z \cosh\left(\frac{k_w x}{\sqrt{2}}\right)\sinh\left(\frac{k_w y}{\sqrt{2}}\right)\right\} \tag{15}$$

and the flat-pole-face wiggler (FPF) is expressed as

$$\mathbf{B}_w = B_w\left[\hat{\mathbf{e}}_y \cosh(k_w y)\sin(k_w z) + \hat{\mathbf{e}}_z \sinh(k_w y)\cos(k_w z)\right]. \tag{16}$$

Multiple segmented wigglers can be easily represented using these models, where the fringe fields are treated in an approximate form. The quadrupole field is defined by using the sharp-edge model

$$\mathbf{B}_Q = \frac{B_Q}{a}(y\hat{\mathbf{e}}_x + x\hat{\mathbf{e}}_y), \tag{17}$$

where B_Q is the magnetic field at the pole tip of the quadrupole and a is the quadrupole aperture radius. The dipoles are defined as $\mathbf{B}_D = B_D\hat{\mathbf{e}}_y$, over some length as defined in the input.

As given above, the electron dynamics are governed by the three-dimensional Lorentz force equations. Although Maxwell's equations are averaged over the harmonic period, no wiggler averaging is imposed on the electron dynamics. This is a valid assumption since the Lorentz force equations are naturally slowly-varying for frequencies near the natural resonances. As a consequence, MEDUSA imposes the expressions

for the electromagnetic and magnetostatic fields at the position of each electron in the orbit equations as follows:

$$v_z \frac{d}{dz}\mathbf{p} = -e\,\delta\mathbf{E} - \frac{e}{c}\mathbf{v}\times\left(\mathbf{B}_w + \mathbf{B}_Q + \mathbf{B}_D + \delta\mathbf{B}\right), \tag{18}$$

where the wiggler, quadrupole, and additionally imposed corrector magnet fields are given in their native form, and the electromagnetic field is determined by the Gauss-Hermite modes. Note that we must take enough steps through the wiggler to resolve the wiggler motion. In practice, we find that ten steps per wiggler period is sufficient.

Finally, it is interesting to note that one can place diagnostics anywhere along the specified undulator line. This includes at the entrance, interior, or exit of a quadrupole magnet, dipole magnet, wiggler, and/or drift space. The current list of diagnostics in MEDUSA now includes:

- the position in meters for each harmonic
- the power in Watts for each harmonic
- the radiation spot size in centimeters for each harmonic
- the curvature of the radiation phase front in radians for each harmonic
- the rms beam radius
- the particle number
- overall efficiency
- energy conservation test
- beam-centroid in the x-direction
- beam-centroid in the y-direction
- average beam-width in the x-direction
- average beam-width in the y-direction
- rms beam radius
- $k_w x$
- $k_w z$
- normalized momentum $p_x / m_e c$
- normalized momentum $p_y / m_e c$
- pondromotive phase in radians
- normalized axial momentum $p_z / m_e c$

3. SIMULATIONS AND COMPARISON TO THE LINEAR THEORY

To test the upgraded MEDUSA, we simulated the APS SASE FEL. This FEL is a proof-of-principle experiment for a possible pathway toward a fourth-generation light source. Although it is capable of radiation wavelength tuning via the electron-beam energy over many wavelengths, the scope of the experiment will include three basic phases: SASE at 517 nm, 120 nm, and shorter. The APS SASE FEL will employ the BNL GUN IV photocathode gun driven by a Nd:Glass laser system;[8] the APS linac, which is capable of producing 650-MeV electrons;[9] and a series of APS Type A fixed gap undulators.[10] Here we will focus only on the simulation of the first experimental phase and have chosen previously achievable electron-beam parameters[11] and the specifications for the undulators. These values may be found in Table 1.

In all of the simulations, we have neglected the wiggler errors. In the first case, we have chosen to represent the undulator beamline as a single-segment parabolic-pole-face wiggler. The actual undulator beamline, however, will be made up of a series of 2.726-m sections, or cells, that are composed of 2.4-m undulators, drift space, diagnostics, and combined-function quadrupole/corrector magnets. In the second case, we represent the undulator line with parabolic-pole-face wigglers. In the third case, we build up the undulator line with flat-pole-face wigglers and the corresponding quadrupoles between these segments. We have chosen to employ a Gaussian beam distribution. Also, to find the optimal wavelength, we performed

wavelength scans at a fixed energy. These results may be found in Figure 1. From this scan, we found the optimum wavelength of 518.819 nm. To verify the performance of MEDUSA in the single-frequency mode, we have found comparable results in the single-segment and multiple-segment cases to simulations performed in RON, GENESIS, GINGER, and TDA3D. All codes also agree well with the linear theory.[12-17] Figure 2 demonstrates the strong correlation of gain length between MEDUSA and the linear theory for various cases of energy spread. The results of the power gain and waist sizes along the length of the undulator for the above three cases, all running in the single-frequency mode, may be found in Figures 3, 4, and 5, respectively. Here we chose to perform these simulations at the resonant wavelength; however, later we will perform multiple harmonic simulations at the optimal wavelength to demonstrate the differences. The four simulations corresponding to Figures 2-5 used an input seed of 10 W, a waist of $w(0)$ = 0.05 cm, three modes, and 5832 particles.

Parameter	Value
Beam Energy	219.5 MeV
Normalized Emittance	5 π mm mrad
Peak Current	150 A
Energy Spread	0.10%
On-Axis Wiggler Strength	10.06 kG
Wiggler Period	3.3 cm
Radiation Wavelength	516.8 nm
Multiple-Segment Case	
Cell Length (includes up and down tapers)	2.726 m
Undulator Length	2.4 m
Quadrupole Length (FPF)	5.0 cm

Table 1: APS SASE FEL Parameters

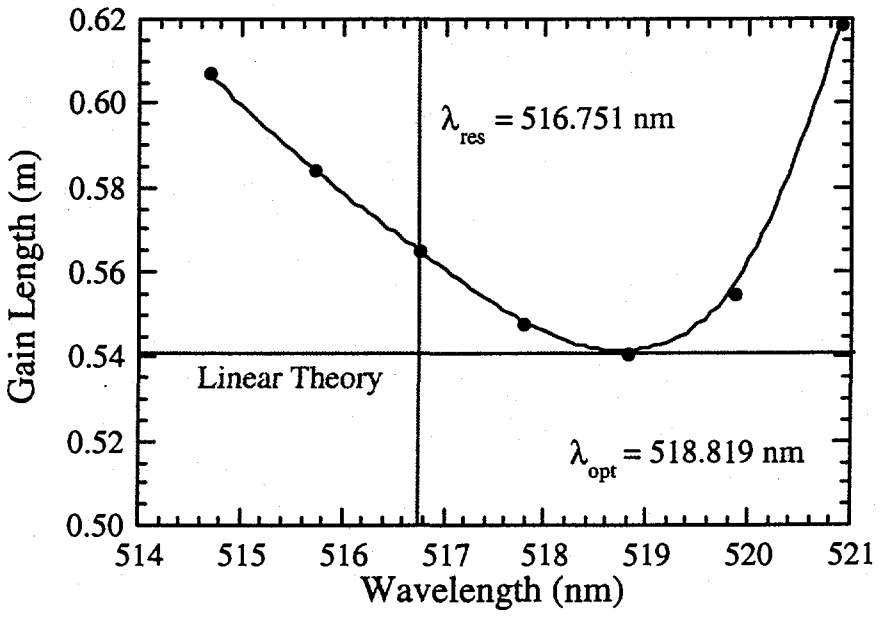

Figure 1: Power versus distance along undulator for wavelength scans at a fixed energy for the single-segment, PPF case.

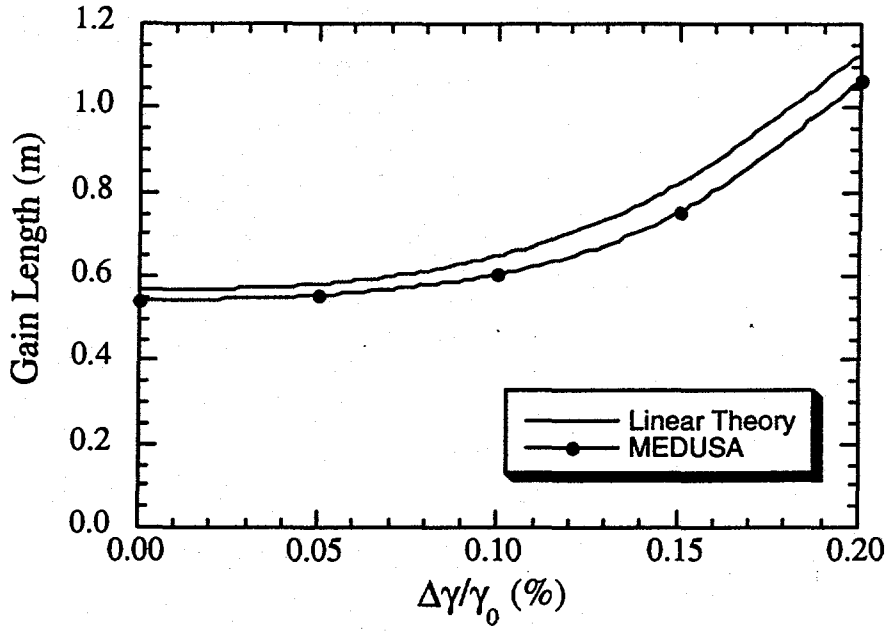

Figure 2: Gain length versus energy spread for the linear theory and the single-segment, PPF case.

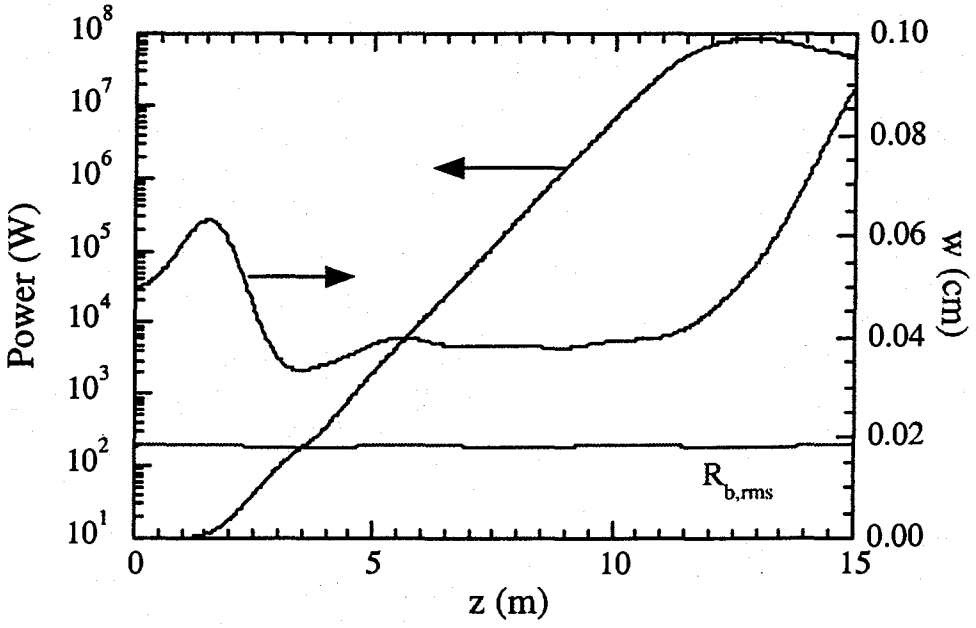

Figure 3: Power at the resonant wavelength, radiation spot-size, and rms beam radius versus distance along the undulator for the single-segment, PPF case.

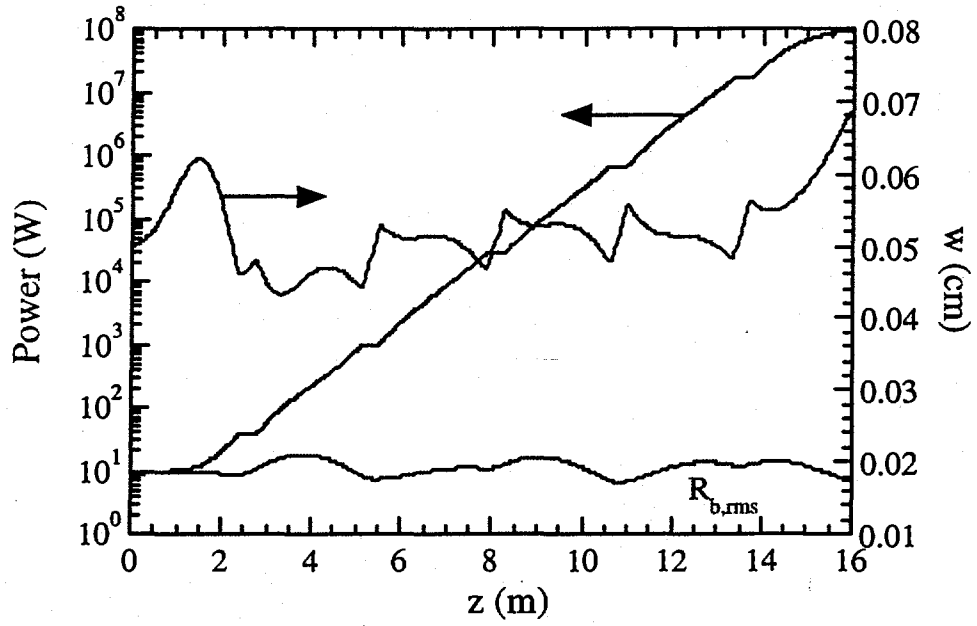

Figure 4: Power at the resonant wavelength, radiation spot-size, and rms beam radius versus distance along the undulator for seven multiple PPF undulators without quadrupoles.

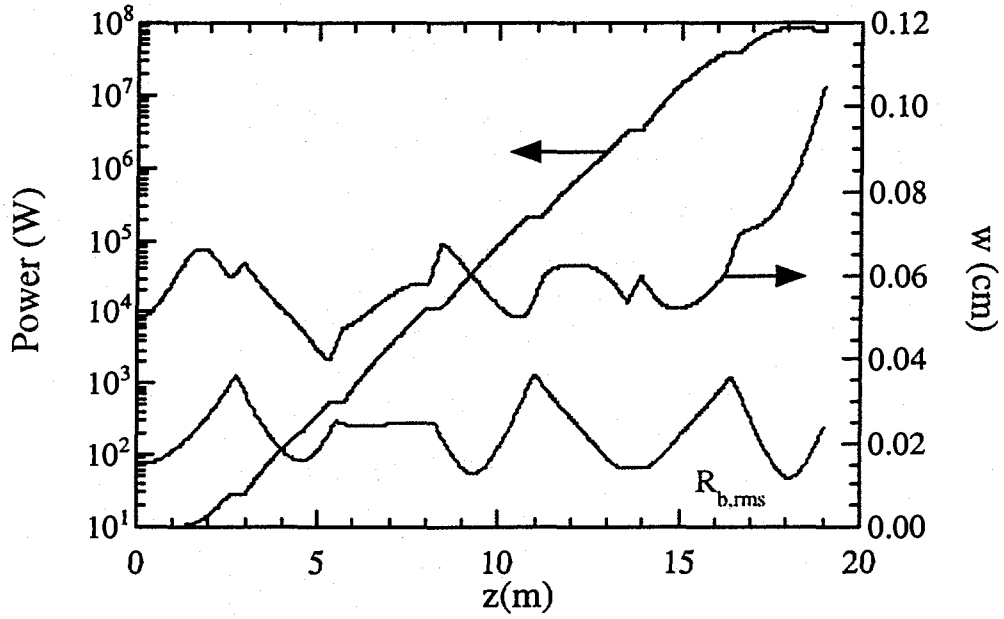

Figure 5: Power at the resonant wavelength, radiation spot-size, and rms beam radius versus distance along the undulator for seven multiple FPF undulators with quadrupoles.

After these initial cases were performed, we further tested MEDUSA by running with multiple harmonics. Again, we performed these simulations with a waist size of $w(0) = 0.05$ cm and a start-up signal of 10 W. We kept the initial waist size constant for each of nine harmonics, but only seeded the fundamental, i.e., the harmonics were allowed to start-up without any input signal. Also, we included a total of 221 modes in all harmonics and 34,992 particles. We performed these simulations for the single- and multiple-segment cases described above. The results of the gain lengths and the harmonic saturation powers for the single-segment PPF case may be found in Table 2. In Figures 6 and 7, the single-segment (PPF) nine-harmonic case is plotted for the odd and even harmonics, respectively. In Figures 8 and 9, the multi-segment (PPF) nine-harmonic case is plotted in the same fashion as the single-segment case. The power in the harmonics is quite significant.

Harmonic Number	Wavelength (nm)	Gain Length (m)	Harmonic Saturation Power
1	516.8	0.592	118 MW
2	258.4	0.335	4.28 kW
3	172.3	0.201	999 kW
4	129.2	0.165	1.57 kW
5	103.4	0.124	47.5 kW
6	86.13	0.098	220 W
7	73.82	0.089	43.5 kW
8	64.59	0.065	144 W
9	57.42	0.072	32.9 kW

Table 2: Variation in gain length and output power with harmonic number in the single-segment, PPF case

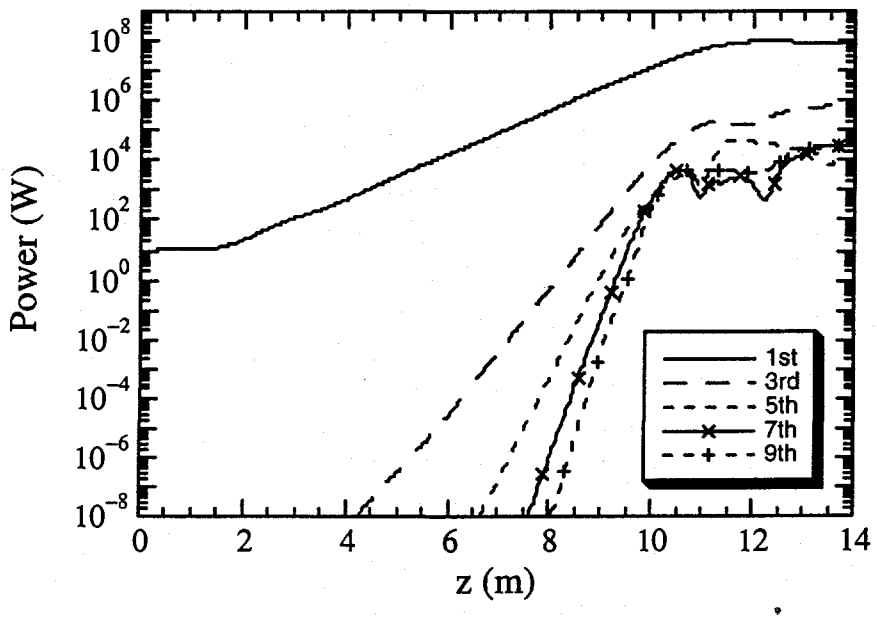

Figure 6: Power versus distance along the undulator for the fundamental and odd harmonics in the single-segment, PPF case. The simulation was run at the optimal wavelength.

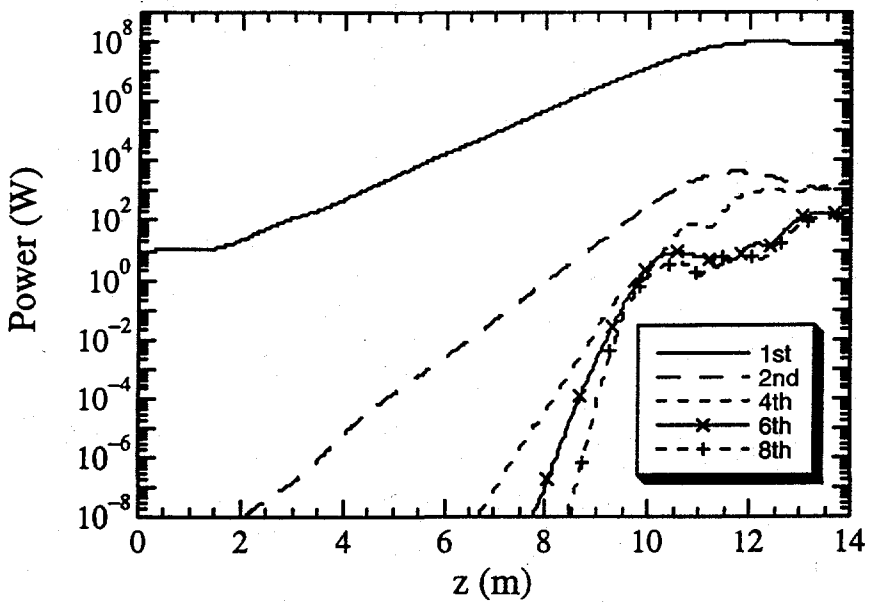

Figure 7: Power versus distance along the undulator for the fundamental and even harmonics in the single-segment, PPF case. The simulation was run at the optimal wavelength.

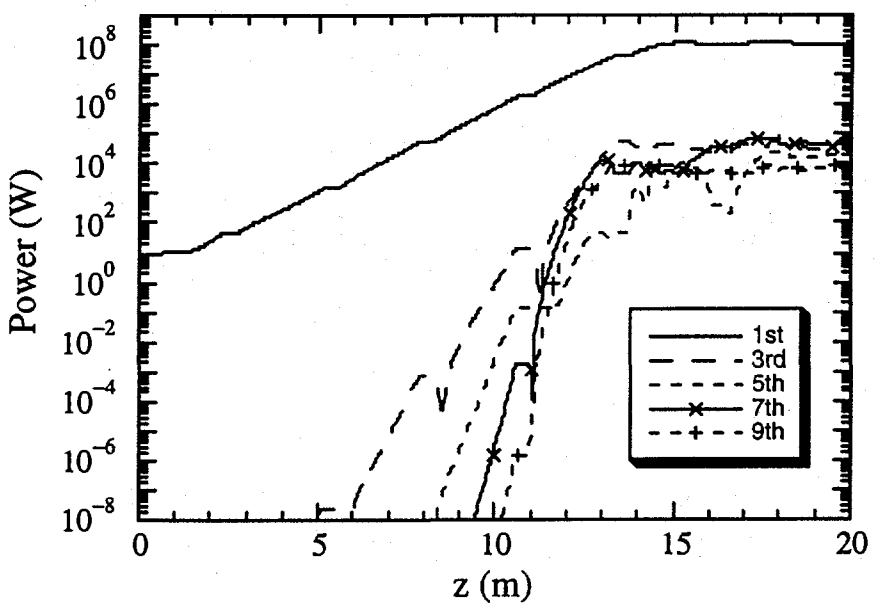

Figure 8: Power versus distance along the undulator for the fundamental and odd harmonics in the multiple-segment, PPF case. The simulation was run at the optimal wavelength.

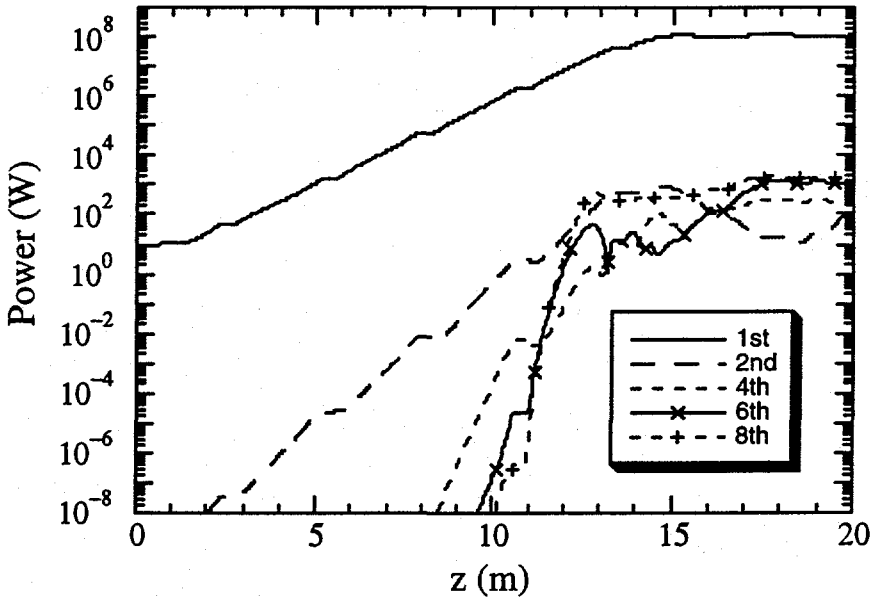

Figure 9: Power versus distance along the undulator for the fundamental and even harmonics in the multiple-segment, PPF case. The simulation was run at the optimal wavelength.

It is interesting to note that not only are the harmonic powers quite high but the harmonic power arises purely from the interaction of the fundamental with the nonlinear component of the source-current. This nonlinear term occurs due to the beam micro-bunching. As seen in Table 2 and Figures 6-9, the gain length varies approximately as $L_G \propto (2h\Gamma)^{-1}$, which is characteristic of this nonlinear component. The scaling of the nonlinear gain-length decreases linearly with the harmonic number, whereas the linear gain lengths increase with harmonic number. This phenomenon has been previously seen in traveling-wave tubes. Notice also in Table 2 and Figures 6-9 (7 and 9 specifically) that the even harmonics do not experience as high a power as compared with the odd harmonics. This is due to the fact that the natural electron motion in the parabolic-pole-face-wiggler configuration does not lead to extraordinary interactions at these even superpositions.

We have also exercised the added beam diagnostic portions of the upgraded MEDUSA. For the two parabolic harmonic runs, single and multi-segmented (both PPF), it is interesting to observe the mode waist along the length of the wiggler and to exemplify the existence of optical guiding only in the fundamental. This may be found in Figures 10 and 11, respectively. This diagnostic as well as those described above will become mandatory for examination of such things as bunching in a high-gain harmonic generation experiment, as is briefly described in the next section.

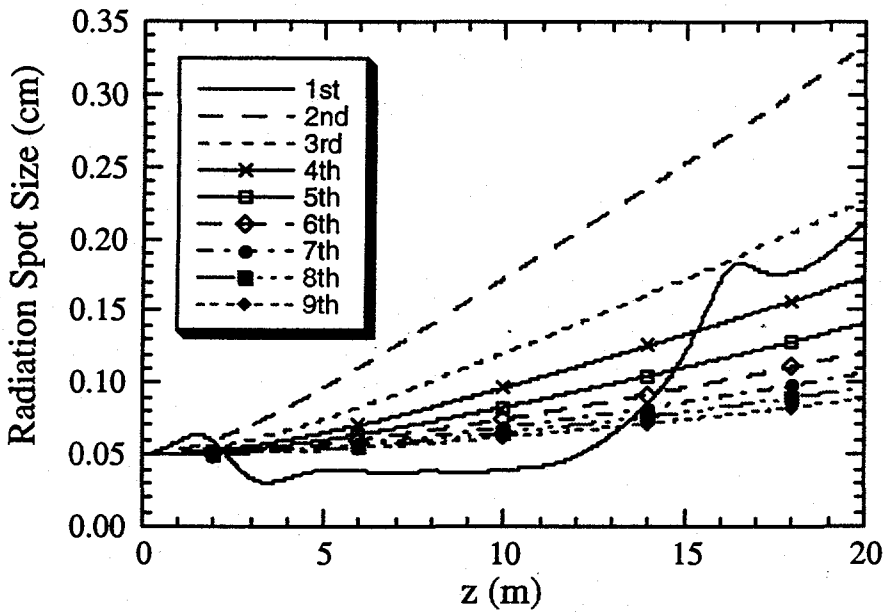

Figure 10: Mode waist versus distance along the undulator for the first nine harmonics in the single-segment, PPF case. The simulation was run at optimal the wavelength.

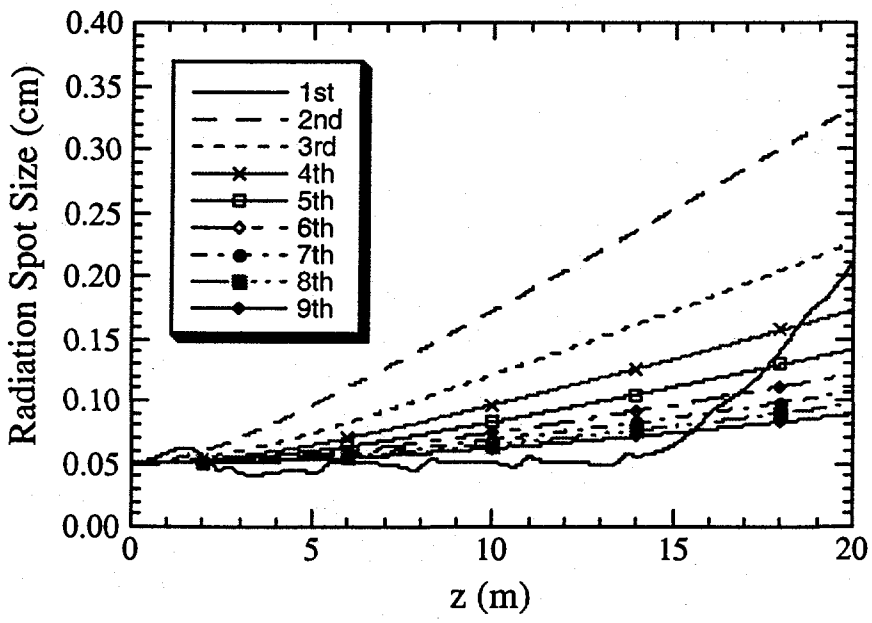

Figure 11: Mode waist versus distance along the undulator for the first nine harmonics in the multi-segment, PPF case. The simulation was run at the optimal wavelength.

4. CONCLUSIONS AND FUTURE PLANS

A three-dimensional code has been developed to handle Gaussian and waterbag distributions, energy spread, multiple-segment wigglers (with the capability of using different wiggler periods, if desired) multiple-frequencies (harmonics and bandwidth), as well as quadrupole focusing and dipoles. With this modified version of MEDUSA, we have simulated the APS SASE FEL, a proof-of-principle experiment for a fourth-generation light source, and have shown the existence of nonlinear harmonic generation. We have found MEDUSA to be in good agreement to other existing FEL codes and to the linear theory.

Future plans for MEDUSA include simulation of another possible pathway to a fourth-generation light source, the high-gain harmonic generation experiment defined in reference 4. In this experiment an electron beam and seed-laser beam, whose wavelength is at the fundamental, pass simultaneously through a first wiggler for energy modulation (the modulative section). Just after this first wiggler is a dispersive section made up of a dipoles chicane that induces bunching, i.e., a longitudinal phase-space rotation. The final step in this process involves a second wiggler (the radiative section), which is in resonance with the electron beam energy and the second harmonic of the input seed radiation. We also plan to complete similar simulation runs with the inclusion of a tapered radiative section. Also, the ability to run with a bandwidth defined around each harmonic will be included in both of the above cases.

Finally, we plan to further upgrade the code with the following options:

- off-axis injection into the first wiggler and between wigglers using "automated" corrector magnets
- inclusion of the spontaneous radiation for the given parameters
- output in APS-standard self-describing data set (SDDS) format, for easy manipulation using the Unix platform[18]
- short beam-pulse interactions
- preprocessor for making multiple sequential runs and corresponding repetitive changes to the input file parameters and the output data file names

ACKNOWLEDGEMENTS

This work was supported by the U.S. Department of Energy, Office of Basic Energy Sciences, under Contract No. W-31-109-ENG-38.

Special thanks to Li-Hua Yu and John Nicolas Galayda for encouraging me (SGB) to perform this work.

REFERENCES

1. H.D. Nuhn, "Comparison of FEL Codes" Proceedings, this conference.
2. H.P. Freund and T.M. Antonsen, Jr., *Principles of Free-electron Lasers* (Chapman & Hall, London, 1986), 2nd edition; H.P. Freund, Phys. Rev. E **52**, 5401 (1995).
3. S.V. Milton et al., "FEL Development at the APS: The APS SASE FEL", Proceedings, this conference.
4. L.H. Yu, Phys. Rev A **44**, 5178 (1991); I. Ben-Zvi et al., Nucl. Instrum. Meth. **A318**, 208 (1992).
5. H.P. Freund, S.G. Biedron, and S.V. Milton, "Nonlinear Harmonic Generation in Free-Electron Lasers," submitted to Physical Review Letters 13 January 1999.
6. L.H. Yu, Phys. Rev A **44**, 5178 (1991).
7. P. Sprangle et al., Phys. Rev. A **36** , 2773 (1987).
8. S.G. Biedron, G.A. Goeppner, S. Pasky, G. Travish, X.J. Wang, et al., "The Operation of the BNL Gun-IV Photocathode RF Gun at the Advanced Photon Source," to be published.
9. M. White, N. Arnold, W. Berg, A. Cours, R. Fuja, A.E. Grelick, K. Ko, Y.L. Qian, T. Russell, N. Sereno, and W. Wesolowski, "Construction, Commissioning and Operational Experience of the

Advanced Photon Source (APS) Linear Accelerator," Proceedings of the XVIII International Linear Accelerator Conference, Geneva, Switzerland, 26-30 August, 1996, pp. 315-319 (1996).
10. S.V. Milton et al., Nucl. Instrum. Meth. **A407**, 210 (1998).
11. M. Babzien, I. Ben-Zvi, P. Catravas, J-M. Fang, T.C. Marshall, X.J. Wang, J.S. Wurtele, V. Yakimenko, and L.-H. Yu, Phys. Rev. E **57**, 6039 (1998).
12. S.G. Biedron, Y.C. Chae, R. Dejus, H.P. Freund, and S.V. Milton, "The APS SASE FEL: Modeling and Code Validation," to be published.
13. R.J. Dejus et al., "An Integral Equation Based Computer Code for High Gain Free-Electron Lasers," in NIM Proceedings of the 20th International FEL Conference (FEL98), Williamsburg, VA, USA, 1998.
14. S. Reiche, "GENESIS 1.3 – A Fully 3D Time Dependent FEL Simulation Code," in NIM Proceedings of the 20th International FEL Conference (FEL98), Williamsburg, VA, USA, 1998.
15. W.M. Fawley, "An Informal Manual for GINGER and its post-processor XPLOTGIN," LBID-2141, CBP Tech Note-104, UC-414, 1995.
16. T.M. Tran and J.S. Wurtele, "TDA – A Three-Dimensional Axisymmetric Code for Free-Electron Laser (FEL) Simulation," in Computer Physics Communications **54**, 263-272 (1989); S. Reiche and B. Faatz, "Upgrade of the Simulation Code TDA3D," in NIM Proceedings of the 20th International FEL Conference (FEL98), Williamsburg, VA, USA, 1998.
17. L.H. Yu et al., Phys. Rev. Lett. **64**, 3011 (1990); M. Xie, in Proceedings of the IEEE 1995 Particle Accelerator Conference, p. 183, 1995.
18. SDDS Reference: M. Borland, "Applications Toolkit for Accelerator Control and Analysis," Proceedings of the IEEE 1997 Particle Accelerator Conference, Vancouver, BC, Canada, p. 2487-2489, 1998.